Journal of Magnetism and Magnetic Materials 324 (2012) 1837–1844

Contents lists available at SciVerse ScienceDirect

Journal of Magnetism and Magnetic Materials

journal homepage: www.elsevier.com/locate/jmmm

Inverse TMR in a nominally symmetric CoFe/AlO_x/CoFe junction induced by interfacial Fe_3O_4 investigated by STEM-EELS

Fengyuan Shi [a,*], Hua Xiang [a], J. Joshua Yang [a,b], M.S Rzchowski [c], Y.A. Chang [a], P.M. Voyles [a]

[a] Department of Materials Science and Engineering and Materials Science Program, University of Wisconsin-Madison, Madison, WI 53706, USA
[b] Quantum Science Research, Hewlett-Packard Laboratories, 1501 Page Mill Road, Palo Alto, CA 94304, USA
[c] Department of Physics, University of Wisconsin-Madison, Madison, WI 53706, USA

ARTICLE INFO

Article history:
Received 11 September 2011
Received in revised form
19 December 2011
Available online 17 January 2012

Keywords:
Magnetic tunnel junction (MTJ)
STEM EELS
Inverse TMR

ABSTRACT

We have found inverse tunneling magnetoresistance (TMR) with a non-symmetric bias voltage dependence in a nominally symmetric Si (001)/Ag/CoFe/AlO_x/CoFe/IrMn/Ag magnetic tunnel junction after field cooling. The O K edge fine structure extracted from electron energy loss spectroscopy spectrum images taken at the interfaces of junctions with inverse TMR shows a thin, discontinuous Fe_3O_4 layer at the CoFe/AlO_x interfaces. The Fe $L_{2,3}$ edge core level shifts are also consistent with those of Fe_3O_4. We find no Fe_3O_4 layer in junctions with normal TMR. We believe this Fe_3O_4 layer is responsible for the inverse TMR.

1. Introduction

Magnetic tunnel junctions (MTJs) consist of two ferromagnetic electrodes separated by an insulating tunnel barrier. MTJs exhibit large changes of the tunneling magnetoresistence (TMR) depending on the relative configurations of the magnetization in the ferromagnetic electrodes. Applications of MTJs include nonvolatile magnetic random access memory (MRAM) elements, hard disk read head sensors, large arrays of sensors for imaging, and ultralow field sensors [1,2].

TMR can be described by Julliere's model [3], in which $TMR=2P_1P_2/(1-P_1P_2)$ where P_1 and P_2 are the spin polarizations of the two ferromagnetic electrodes. P is defined as $[D_\uparrow(E_F)-D_\downarrow(E_F)]/[D_\uparrow(E_F)+D_\downarrow(E_F)]$, in which $D_\uparrow(E_F)$ and $D_\downarrow(E_F)$ are the densities of states (DOS) of the electrode at the Fermi energy (E_F) for the majority-spin and minority-spin bands, respectively, defined with respect to the electrode magnetization [4]. From the TMR definition in Julliere's model, when P_1 and P_2 have the same sign, the TMR is positive, which is called normal TMR. When P_1 and P_2 have the opposite signs, so the tunneling current from one electrode is dominated by minority spins, the TMR signal is negative and called inverse TMR.

Inverse TMR can be caused by either the intrinsic spin polarization of the ferromagnetic electrodes or spin dependent tunneling of the entire ferromagnetic electrode/tunnel barrier system. Ferromagnetic materials with negative intrinsic spin polarization include Fe_3O_4 [5] and Fe_4N [6]. If a junction is formed with one negative polarization electrode, one positive polarization electrode, and a barrier that enables tunneling of the spin band that dominates the polarization, the TMR will be negative. One such structure is Fe_4N/MgO/CoFeB [7]. However, the tunnel barrier can have a dramatic influence on which electrode states contribute to the tunneling current. For example, Co has negative intrinsic spin polarization of the d-like band at E_F [8], but an AlO_x barrier favors tunneling of s-like states, so the tunneling spin polarization at the Co/AlO_x interface is positive [9,10]. Thus, a Co/AlO_x/$La_{0.7}Sr_{0.3}MnO_3$ junction has positive TMR [8]. $SrTiO_3$ favors d-like tunneling so the Co/$SrTiO_3$ interface gives negative tunneling spin polarization, and a Co/$SrTiO_3$/LSMO junction has negative TMR [8,11]. Another example of inverse TMR is a NiFe/Ta_2O_5/AlO_x/NiFe double barrier junction, in which NiFe/Ta_2O_5 favors negative spin polarized tunneling and AlO_x/NiFe favors positive spin polarized tunneling [12,13]. Inverse TMR has also been induced in devices with more complicated structures, such as MTJs with two tunnel barriers and two pinned electrodes [14].

CoFe/AlO_x/CoFe MTJs have been extensively studied [15–22], and almost all of them exhibit normal TMR. Du et al. [15] observed inverse TMR in a CoFe/AlO_x/CoFe junction if they over-oxidized when transforming a thin Al film into the AlO_x tunnel barrier. They speculated that Fe_3O_4 formed at the interface, but did not present any data supporting this hypothesis. Yang et al. [22] showed that XPS from an over-oxidzed CoFe/AlO_x interface (the bottom half of a junction) exhibited Fe^{3+} and Fe^{2+} peaks typical of Fe_3O_4.

Here, we use aberration-corrected high resolution scanning transmission electron microscopy (HRSTEM) and STEM electron

* Corresponding author.
E-mail addresses: fshi4@wisc.edu (F. Shi), voyles@engr.wisc.edu (P.M. Voyles).

0304-8853/$ - see front matter © 2012 Elsevier B.V. All rights reserved.
doi:10.1016/j.jmmm.2012.01.012

energy loss spectroscopy spectrum imaging (STEM EEL SI) to investigate both interfaces of full CoFe/AlO_x/CoFe MTJs. We compare three types of junctions: (1) CoFe/AlO_x/CoFe MTJs deposited on an Ag buffer layer on Si, which exhibit inverse TMR after field cooling; (2) the same MTJs, which exhibit normal TMR before field cooling; and (3) CoFe/AlO_x/CoFe deposited on a TiN buffer, which exhibit normal TMR, both before and after field cooling. Based on the O K-edge electron energy loss near-edge structure (ELNES) [23] and the Fe $L_{2,3}$ edge core level shifts [24], both CoFe/AlO_x interfaces in the inverse TMR junctions have some regions covered with Fe_3O_4. EELS SI shows that the Fe_3O_4 is not a continuous film, and as a result, it is not visible as a distinct layer in the HRSTEM images. We find no Fe_3O_4 in the normal TMR junctions, although some other Fe oxides are present, so we ascribe the inverse TMR to negative spin polarized tunneling from Fe_3O_4.

2. Material and methods

The normal TMR junctions in this study consisted of Si (001)/TiN (001) (9 nm)/$Co_{75}Fe_{25}$ bcc (001) (20 nm)/AlO_x tunnel barrier (1.7–2 nm)/$Co_{75}Fe_{25}$ (5 nm)/$Ir_{22}Mn_{78}$ (20 nm)/Ag (100 nm). The TiN buffer was reactively sputtered in 6 mTorr Ar and 0.5 mTorr N_2 mixture at a substrate temperature of 550 °C. The bottom epitaxial $Co_{75}Fe_{25}$ electrode was sputtered on the TiN buffer in 6 mTorr Ar at room temperature (RT) and then annealed *in situ* at 400 °C for 10 min. After the substrate cooled to RT, the AlO_x tunnel barrier was formed by rf sputtering of 1.2 nm of Al metal followed by *in situ* rf plasma oxidation in 100 mTorr of oxygen. The top polycrystalline $Co_{75}Fe_{25}$ electrode, IrMn, and Ag layers were sputtered in 6 mTorr Ar at RT. The inverse TMR samples have a similar structure deposited under the same conditions, but with an Ag bottom buffer layer deposited at RT sputtering in 6 mTorr Ar instead of a TiN buffer layer. The complete structure of these samples is Si (001)/Ag fcc (001) (35 nm)/$Co_{75}Fe_{25}$ bcc (001) (20 nm)/AlO_x (1.7–2 nm)/$Co_{75}Fe_{25}$ (5 nm)/$Ir_{22}Mn_{78}$ (20 nm)/Ag (100 nm). Junctions were studied in the as-deposited state and after field cooling, which was carried out in air by annealing the sample at 200–300 °C for 2 min and then cooling to RT under a 1000 Oe magnetic field. Some MTJ sheet films were patterned into round junctions with radii ranging from 55 to 95 μm by photolithography and Ar ion milling. Transport measurements were carried out using the standard dc four-probe method. The transport properties of the junctions were all measured at room temperature.

The TEM/STEM samples were prepared by tripod polishing following the steps used by Voyles et al. [25], followed by final thinning by ion milling for 1 h in a Fischion 1010 with ion beam energy 5 kV and 5 mA current. Before going into the microscope, to avoid contamination the samples were plasma-cleaned for 3 min with 25% O_2+Argon (balanced) at 22 psi with a Fischion plasma cleaner model 9020.

HRSTEM and STEM EELS were performed in a FEI Titan STEM with CEOS probe aberration corrector operated at 200 kV. For imaging we used high-angle annular dark-field (HAADF) Z-contrast STEM, with collection angles of 67–337 mrad, probe convergence angle of 24.5 mrad, and probe current of $\sim$25 pA, resulting in spatial resolution <0.1 nm. The EEL SIs were taken in EFSTEM mode with camera length CL=248 mm, convergence angle of 17.5 mrad, probe current 100 pA, spatial resolution $\sim$0.1 nm, and EELS collection angle $\beta=53$ mrad. The smaller convergence angle was used to reduce the probe current, which was necessary to avoid beam damage to the specimens. It also generates a more compact probe for microanalysis. The SIs were acquired on a GIF 865, with energy dispersion of 0.2 eV/pixel, and energy resolution of 0.8 eV. The SIs were processed by weighted principal component analysis (weighted PCA) for de-noising [26,27]. In this experiment, 30 principal components were used to maintain the energy loss near edge fine structures (ELNES). This relatively large number of principal components was required due to correlated noise in the spectrum image from imperfect gain normalization and dark subtraction.

Composition profiles were extracted from the corresponding EEL SIs and then integrated horizontally along the junctions. Quantifications were calculated without PCA using the DigitalMicrograph implementation of the standard quantification method [28]. We assumed the horizontal compositions were uniform for all the junctions, which is true for an SI with a small field of view along the interface and a small drift rate perpendicular to the interface. The reference for measurement of Fe $L_{2,3}$ core level shifts is an artifact peak in the EELS around 700 eV, which is due to secondary emission from the Titan Schottky emission gun. This artifact peak is material independent, but captures fluctuations in the high voltage, spectrometer prism current, and lab EM fields, so it provides us a reliable reference from which to determine the Fe $L_{2,3}$ core level shifts.

3. Results

Fig. 1 shows TMR loops and bias dependences for the TiN-buffered, 250 °C field-cooled junction (a) and (b), the as-prepared, Ag-buffered junction (c) and (d), and the Ag-buffered, 300 °C field-cooled junction (e) and (f). The TiN-buffered junction shows relatively high normal TMR signal (65%) with symmetric bias dependence. The as-deposited, Ag-buffered junction also shows normal TMR with symmetric bias dependence, although it is lower, about 11% at room temperature under 0.035 V bias voltage. Only the Ag-buffered, field-cooled junction shows inverse TMR. Its TMR is about -7% under -0.3 V bias voltage, and the TMR bias dependence is asymmetric.

Fig. 2 shows HRSTEM images of all three junction structures. Each image shows, from top to bottom, the IrMn, CoFe, AlO_x, and CoFe layers. The Ag or TiN buffer layer and the Si substrate are not shown. There are no obvious second phase layers visible in these images. At a flat interface, continuous layers as thin as a monolayer are visible using this technique [29–31]. The CoFe/AlO_x interfaces have some roughness [20], but even nearly atomically flat local regions in the images have no second phase. However,

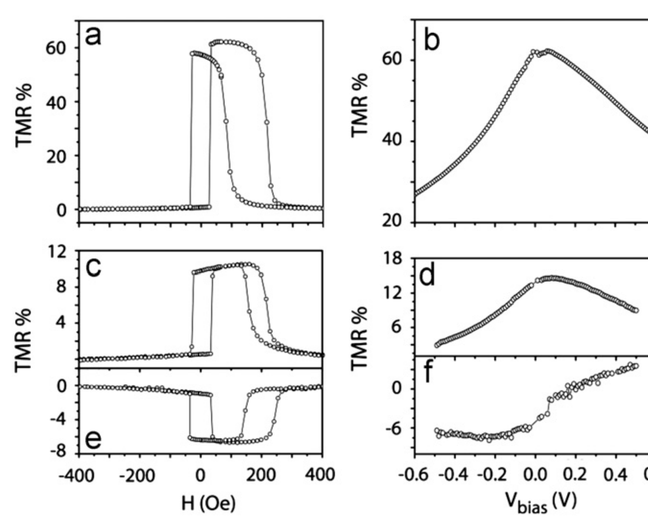

Fig. 1. TMR loops and bias dependence for (a) and (b), a TiN-buffered, 250 °C field-cooled junction, (c) and (d), an as-prepared Ag-buffered junction, and (e) and (f), a Ag-buffered, 300 °C field-cooled junction. Only (e) and (f) show inverse TMR.